ADVANCED FUNCTIONAL MATERIALS
www.afm-journal.de

Europium-Based Metal–Organic Framework with N—H···π Interaction and Intramolecular Energy Transfer Mechanisms for Self-Electrochemiluminescence

Lu Zhao, Xiang Ren, Yu Du, Zhongfeng Gao, Hongmin Ma, Huan Wang, Yuyang Li, Qin Wei, Huangxian Ju,* and Dan Wu**

This work proposes a europium-based metal–organic framework ($[Eu_2(HNCP)_4Cl_4(H_2O)_2]_n$, named ZL-1), featuring dinuclear $Eu_2(COO)_2$ clusters as connecting nodes, linked by benzimidazolyl tridentate ligand 2-(4-carboxyphenyl)-imidazo[4,5-f]-1,10-phenanthroline (HNCP) for efficient self-electrochemiluminescence (self-ECL). The cathodic ECL emission shows two peaks with a maximum intensity of 7500 a.u.at 0 ~ −1.8 V in pH 9.0 phosphated buffered solution (PBS) without extra coreactant. The cleavage of N—H bond in benzimidazolyl group can occur under alkaline conditions to generate neutral radical ZL-1•. After applying voltage, the ZL-1 can be reduced twice to form ZL-$1_{Re1}^{\bullet-}$ and ZL-$1_{Re2}^{\bullet-}$. Then, ZL-$1_{Re1}^{\bullet-}$ and ZL-$1_{Re2}^{\bullet-}$ react with ZL-1•, accompanied by transferring energy from HNCP to central Eu^{3+} to produce excited ZL-1_{Re1}* and ZL-1_{Re2}* for ECL1 and ECL2 emissions. The local excitation in the HNCP unit is demonstrated with cyclic voltammetry (CV) and stepping pulse ECL. The stimulated and luminous species are confirmed by density functional theory calculations and ECL spectra. This design approach of self-ECL materials, which coordinated functional ligands with lanthanide metal ions as 3D-structured MOF, broadened the applications of ECL systems to loose conditions and facilitated mechanistic exploration of ECL processes.

1. Introduction

Powered by the applied voltage, a redox-induced light is emitted via electron transition from the excited state to the ground state of the luminophore, which leads to electrochemiluminescence (ECL) output signal.[1–3] The ECL technique has attracted tremendous attention in clinical diagnosis, drug screening, food and environment detection with merits of low background, wide dynamic ranges, and plain operation.[4–7] Importantly, the performance of the luminophore plays a decisive role in the efficiency of ECL devices. Luminophores are divided into self-electrochemiluminescence (self-ECL) type and coreactant auxiliary type.[8] Although the latter occupies the majority,[9] the eminent bottleneck remains in low efficiency of intermolecular electron transfer between the coreactant and luminophore because they exist in different phases, thus leading to poor stability, the higher cost, low ECL signal, and sensitivity.[10,11] By contrast, the luminophore with efficient self-ECL can avoid these problems very well to realize strong ECL.

Nowadays, metal-organic frameworks (MOFs) are quite popular in various fields because of their self-assembly properties, which make them synthesize purposefully to meet different application needs.[12–16] Thus some efficient self-ECL MOFs have been designed by using organics with luminescence or annihilation properties as ligands.[10,17,18] At present, there are a few reports on the synthesis of self-ECL type MOF by this strategy. For example, an annihilation Zn-MOF has been synthesized by utilizing 4′-(4-carboxyphenyl)−2, 2′:6′, 2″-terpyridine (Hcptpy) as the organic luminescence ligand and zinc as the metal node, achieving the dual-signal ECL.[17] Eu-MOFs, a member of Ln-MOFs, have showed great advantages in applications related to luminescence.[19,20] Ln-MOFs own intrinsic luminescence preponderance (such as lofty luminescent efficiency, long lifetime, and immanent narrow emission peak) by virtue of affluent ladderlike electronic levels and 4*f*-4*f* transitions. In addition, the unique antenna effect of Ln-MOFs can avoid the drawback of the hard directly photo-excitation of Ln ions, thus making Ln-MOFs possess high luminescence.[19–22] Among lanthanide, Eu is more abundant (10^{-6} wt) and the utilization rate is high. Inspired by ECL luminophore in our previous work,[23,24] Eu-MOFs have excellent performances. Therefore, using suitable ligands and

L. Zhao, X. Ren, Z. Gao, H. Ma, H. Wang, Y. Li, Q. Wei, H. Ju, D. Wu
School of Chemistry and Chemical Engineering
University of Jinan
Jinan 250022, P. R. China
E-mail: sdjndxwq@163.com; hxju@nju.edu.cn; chm_wud@ujn.edu.cn
Y. Du
School of Water Conservancy and Environment
University of Jinan
Jinan, Shandong 250022, P. R. China
Q. Wei
Department of Chemistry
Sungkyunkwan University
Suwon 16419, Republic of Korea

The ORCID identification number(s) for the author(s) of this article can be found under https://doi.org/10.1002/adfm.202410886

DOI: 10.1002/adfm.202410886

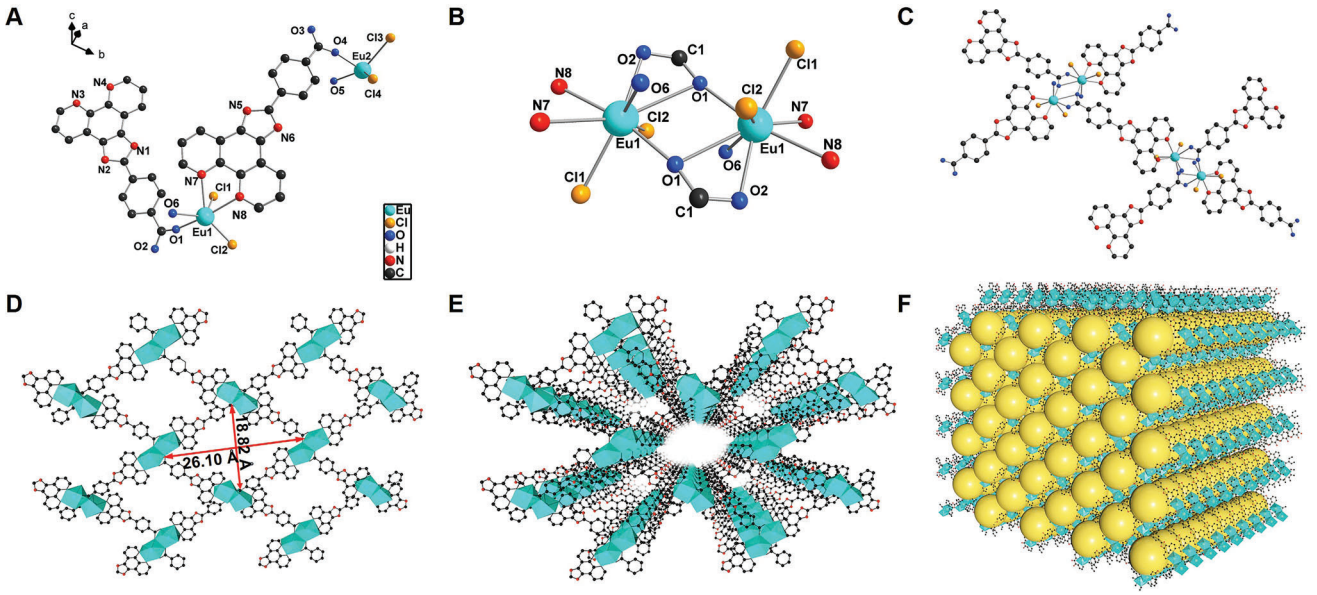

Figure 1. A) Coordination environment of Eu(III) ions in ZL-1 (symmetry codes: #1-x, 1-y, -z). B) Coordination polyhedral geometry of Eu(III) ions. C) Ball-and-stick model of $[Eu_2(COO)_2]$ SBUs in ZL-1. D) 2D layer along the [1-1-1] direction. E) Stick model representation of a single 3D framework viewed along the [1-1-1] direction. F) Crystal structure packed of several multi cells. Atom color scheme: C, black; N, red; O, blue; Cl, orange; Eu, light blue polyhedra. H atoms are omitted for clarity. Yellow balls indicate the space in the framework.

europium ions to self-assemble MOFs is a feasible method for designing and synthesizing self-ECL type luminophore.

Benzimidazole-based organic compounds have unique photophysical properties to generate reactive nitrogen-centered radicals,[25,26] which is a potential to make the synthesized MOF have self-ECL properties. Here, we chose 2-(4-carboxyphenyl)-imidazo[4,5-f]−1,10-phenanthroline (HNCP) as the ligand and synthesized a Eu-MOF named ZL-1 by coordinating with Eu(III) ion. The highly crystallized ZL-1 as ECL luminophore presented good performance with self-luminous model in alkaline medium. Specifically, the good self-ECL performance was obtained through the cleavage of the N—H bond in benzimidazolyl ring to generate neutral radical ZL-1•, the two-step electroreduction to produce ZL-$1_{Re1}^{\bullet-}$ and ZL-$1_{Re2}^{\bullet-}$, the intramolecular electron transfer and energy transfer with an antenna effect from HNCP to central Eu^{3+}. These were rationalized by various experimental characteristics and density functional theory (DFT) calculations. The self-ECL ZL-1 as molecular crystalline material provides a feasible method to design novel luminophores with the simple and controllable synthesis steps for efficient ECL in co-reactant-free conditions.

2. Results and Discussion

Single-crystal X-ray diffraction analysis revealed that ZL-1 has a 3D structure with binuclear units, and crystallizes in the triclinic system with space group P $\bar{1}$ (Table S1, Supporting Information). The asymmetric unit contains two Eu(III) ions, two coordinated NCP^- anion, two coordinated chlorine atom, and two coordinated water molecule (**Figure** 1A). The eight-coordinated Eu(III) ions with the distorted dodecahedron coordination geometries are occupied by four O atoms, two N atoms, and two Cl atoms (Figure 1B), in which two N atoms are from a chelating NCP^- anion and coordinate to one Eu(III) ions [Eu1-N7 = 2.596(4) Å and Eu1-N8 = 2.550(4) Å], four O atoms coordinate to one Eu(III) ion from two μ_3-COO^--bridging NCP^- anions [Eu1-O1 = 2.358(3) Å, Eu1-O1#1 = 2.837(3) Å and Eu1-O2 = 2.431(3) Å] and one water molecule [Eu1-O6 = 2.410(3) Å], the two Cl atoms are derived from the raw material of $EuCl_3$•$6H_2O$ [Eu1-Cl1 = 2.722(14) Å and Eu1-Cl2 = 2.705(13) Å]. The two adjacent Eu(III) ions are doubly bridged by the carboxyl groups from two NCP^- anions to yield a binuclear europium(III) cluster $[Eu_2(COO)_2]$; Figure 1C], and the Eu1···Eu1 and Eu2···Eu2 distances are 4.2891(5) Å and 4.3707(5) Å in the cluster. In the whole ZL-1, the N-Eu1-N and N-Eu2-N bond angles are 63.24(11)° and 63.70(11)°, the Cl-Eu1-Cl and Cl-Eu2-Cl bond angles are 79.21(4)° and 77.38(4)°. The O-Eu-O, O-Eu-Cl, N-Eu-Cl and O-Eu-N bond angles are in the ranges of 47.89(9)−116.77(10)°, 71.70(6)−150.67(7)°, 72.38(8)−140.13(8)° and 72.46(11)−170.97(11)°, respectively. The bond lengths and angles of ZL-1 are in the normal ranges (Table S2, Supporting Information). The $[Eu_2(COO)_2]$ SBUs of ZL-1 interconnect by onefold parallel NCP^- anion to obtain a 2D parallelogram frame along the [1-1-1] direction (Figure 1D). These $[Eu_2(COO)_2]$ SBUs are cross-connected to each other to form an infinite 2D network structure into a 3D framework, and the π-π stacking interactions resulting from the intersection of the coordinated NCP^- anions of the neighboring $[Eu_2(COO)_2]$ SBUs stabilizes the adjacent intersected frameworks (Figure 1E,F).

As shown in Figure S1 (Supporting Information), a maximum of the ECL signal was exhibited when the concentration of ZL-1 reached 80 μM. This phenomenon was because the self-absorption effect of the luminophore caused the suppression of the ECL signal when the luminophore concentration reached a certain value. All tests were conducted under 80 μM of ZL-1 to obtain the optimal ECL performance. In **Figure** 2A, the ECL intensity of the ZL-1-modified glassy carbon electrode (GCE) was

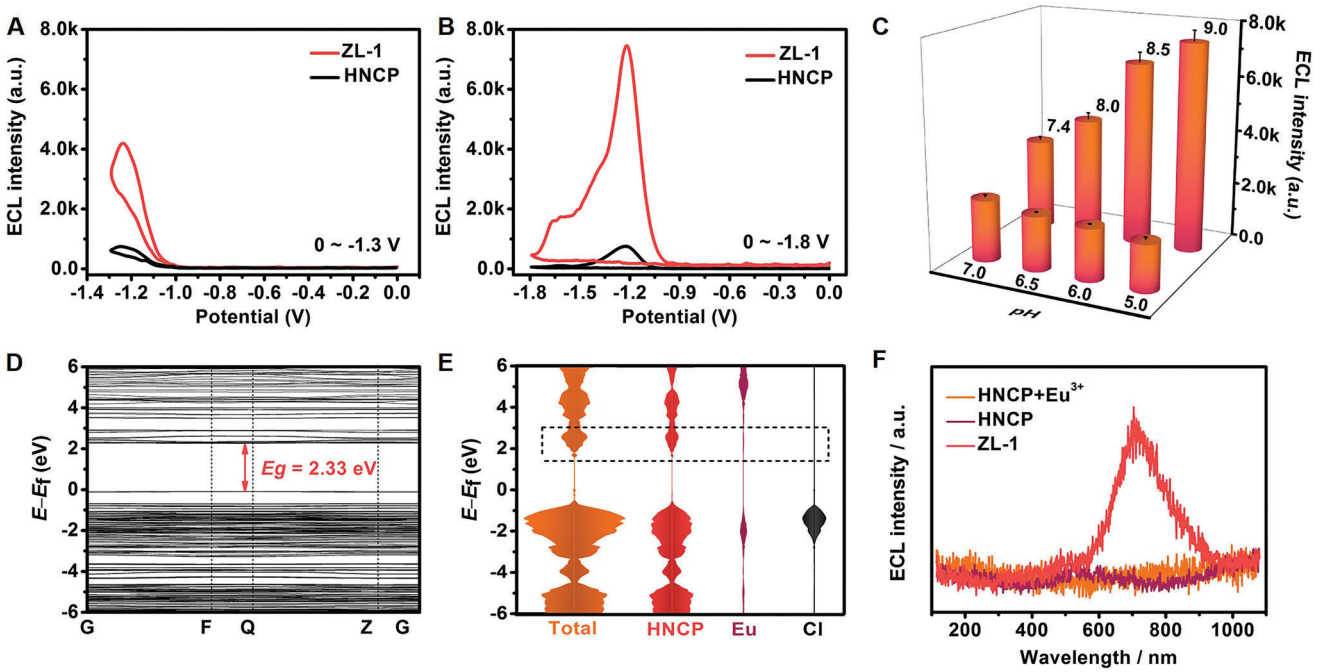

Figure 2. ECL intensity-potential curves of ZL-1-modified GCE and HNCP-modified GCE at A) 0 ~ −1.3 V and (B) 0 ~ −1.8 V under pH 9.0 PBS. (C) ECL intensities of ZL-1-modified GCE under different pH conditions (potential: 0 ~ −1.8 V). Error bars = SD (n = 5). D) Band structure of ZL-1. E) DOS of ZL-1 and LDOS of its components. The main research parts were marked out by the blank dotted square. F) ECL spectra of ZL-1, HNCP, and the mixture of HNCP and Eu^{3+} under pH 9.0 PBS. (The concentrations of ZL-1, HNCP, and Eu^{3+} were all 80 μM).

improved 6.2-fold compared with that of the HNCP-modified GCE. But the GCE loaded the mixture of HNCP and Eu^{3+} showed similar ECL intensity to the HNCP-modified GCE, and the bare Eu^{3+}-modified GCE produced an extremely weak signal (Figure S2, Supporting Information). This phenomenon was caused by the unique framework structure, which eliminated aggregation-caused quenching effects between ligands that would lead to low signal.[27,28] When the range of ECL test was extended to 0 ~ −1.8 V (Figure 2B), the ECL signal of the ZL-1-modified GCE at −1.2 V was further enhanced to 9.7-fold compared with that of the HNCP-modified GCE, and the ECL signal of the HNCP-modified GCE did not change significantly. Meanwhile, a new peak of the ZL-1-modified GCE was observed at about −1.7 V, which attributed to the secondary reduction of ZL-1. In addition, the ECL signals for the GCE loaded the mixture of HNCP and Eu^{3+} and the bare Eu^{3+}-modified GCE has not changed distinctly compared with the test voltage range of 0 ~ −1.3 V (Figure S3, Supporting Information). These led us to realize that the single HNCP ligand was not the source of the ECL1 and ECL2 signals of ZL-1, but its reduction process had played a role in inducing the ECL of ZL-1. Moreover, the ECL intensities were increased under alkaline conditions (Figure 2C; Figure S4, Supporting Information), which demonstrated that some kind of reaction inside the ZL-1 molecule have existed to generate the enhanced ECL components under alkaline conditions.

The fundamental electronic structures of ZL-1 were explored to its luminescent components. The band structures and densities of states (DOS) of different components were obtained via first-principle calculations based on density functional theory (DFT) with generalized gradient approximation (GGA). The calculated bandgap of 2.33 eV was almost consistent with the experimental result of ZL-1 from the UV–vis diffuse-reflectance spectrum (UV-vis DRS, Figure 2D; Figure S5, Supporting Information),[29,30] and the band structures confirmed that the ZL-1 was a semiconductor. For the DOS of ZL-1 and the distribution of local density of states (LDOS) of HNCP, central Eu atom and coordination Cl atom (Figure 2E), the coordination between the Eu^{3+} and the HNCP ligand increased the energy bands near the Fermi level, which meant that the conductivity increased.[31,32] And the contribution above the Fermi energy level (E_f) of ZL-1 mainly originated from the HNCP ligands in the framework. Interestingly, the ECL spectrum of ZL-1 showed a weak broad band centered at 518 nm and a strong band centered at 711 nm (Figure 2F), which was consistent with the reflected situation from the intensity-potential curves. Moreover, no peak was observed in the ECL spectra of bare HNCP and the mixture of HNCP and Eu^{3+}. These demonstrated that HNCP ligand was not the luminescent host of ZL-1.

In order to explore the ECL mechanism, we tested the ECL intensities of the ZL-1-modified GCE in PBS (curves purple) and PBS with extra HNCP (curves orange) under different pH (9.0, 8.0, 7.0, 6.0, and 5.0) respectively. Compared with curves purple in **Figure** 3A–E, the ECL intensities of curves orange were obviously improved. We speculated that the HNCP ligand can prompt the entire ZL-1 to produce some reaction substance that stimulated the generation of ECL. This was because the HNCP was added in the electrolyte separately, rather than modified on the electrode. Therefore, HNCP did not participate in the electrode reaction and did not have the luminophore

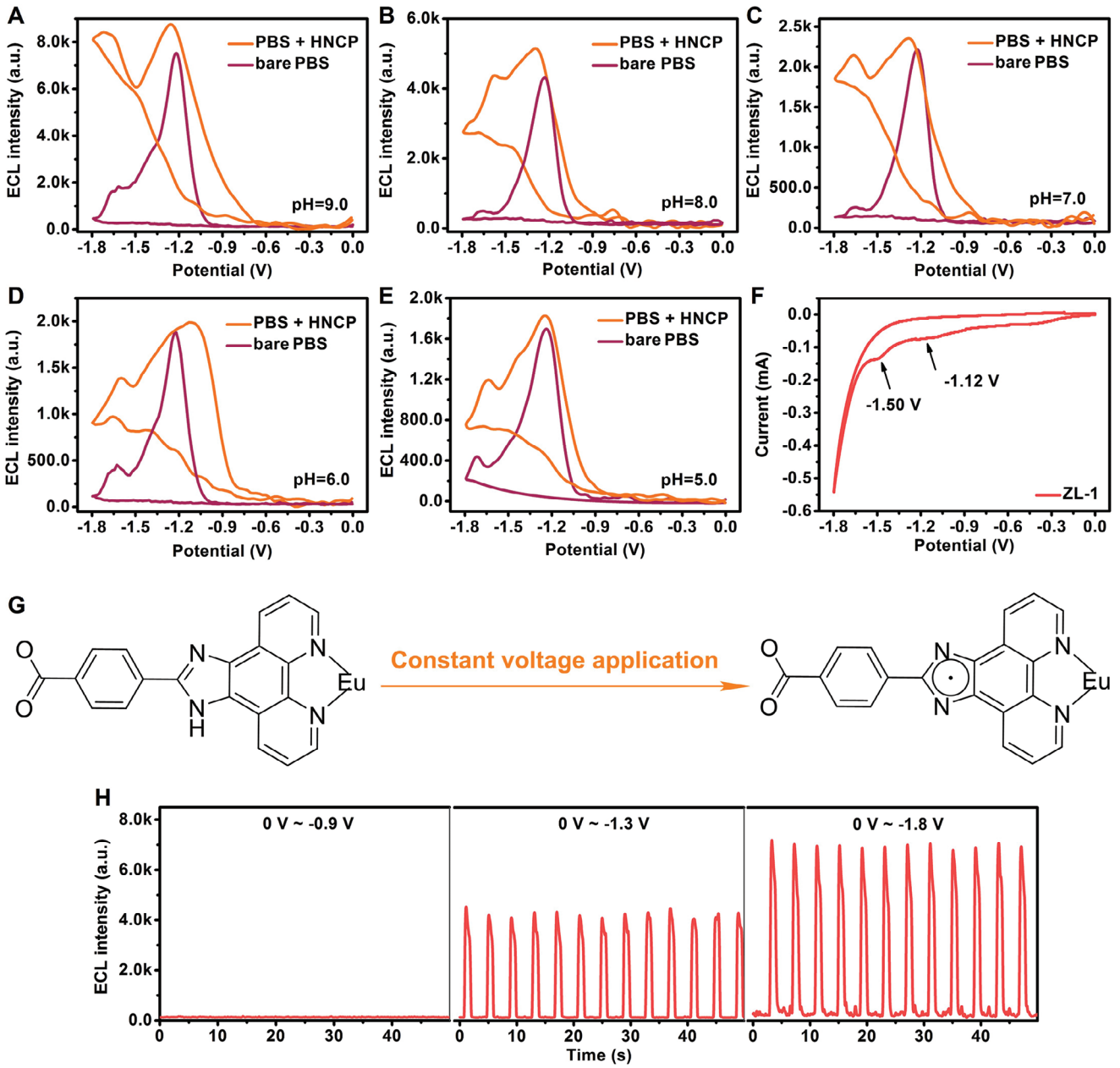

Figure 3. ECL intensity-potential curves of ZL-1-modified GCE under pH A) 9.0, B) 8.0, C) 7.0, D) 6.0, and E) 5.0 (curves purple: in PBS; curves orange: in PBS added 80 μM HNCP). F) CV curves of ZL-1 at 0 ~ −1.8 V under pH 9.0 PBS. G) Mechanism for the formation of neutral radical ZL-1• by N—H bond cleavage under applying constant voltage. H) SP-ECL transients of ZL-1-modified GCE under pH 9.0 PBS from 0 to −0.9, −1.3, and −1.8 V (PMT = 800 V).

characteristic. In order to verify the function of HNCP, the electron paramagnetic resonance experiment with DMPO as radical scavenger was used to explore the production of neutral radical ZL-1•. The obvious peaks were observed in Figure S6 (Supporting Information), which were matched with the reported literature.[33] From the FTIR spectra of ZL-1 before and after ECL measurements (Figure S7, Supporting Information), it was found that the peak strength of N—H bond in benzimidazolyl ring weakened (1076 cm^{-1}) or even disappeared (617 cm^{-1}), indicating that the ZL-1• was produced by the N—H···π interaction in benzimidazolyl ring, which helped the HNCP structure in ZL-1 to form the N-centered (imidazolyl-type) radical via the cleavage of the N—H bond (Figure 3G).[33,34] Combined Figure 2C with Figure 3A–E, ZL-1 exhibited very low ECL signals in acidic and neutral conditions, and showed enhanced ECL performance with the increase of alkaline from pH = 7.0 to 9.0. These indicated that N—H bond cleavage was more likely to occur under alkaline conditions, and due to the electron cloud density characteristics of benzimidazolyl ring, N—H bond was more likely to break in stronger alkaline conditions.

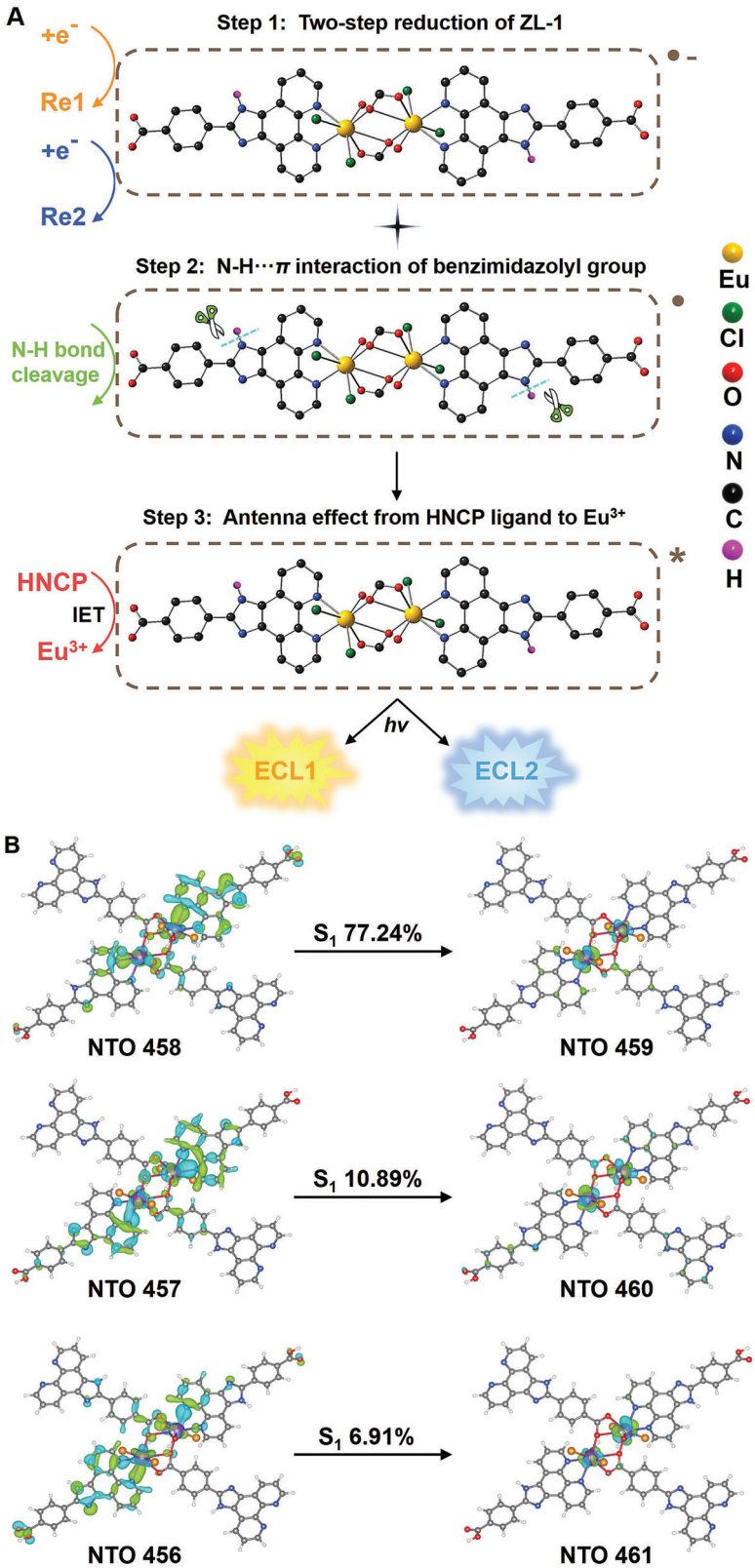

Figure 4. A) Schematic diagram of the self-electrochemiluminescence mechanism via the two-step reduction of ZL-1, the N—H···π interaction of benzimidazolyl group and antenna effect from HNCP ligand to Eu^{3+}. IET: intramolecular energy transfer. B) NTO isodensity surfaces of S_1 for ZL-1 clusters (isovalue = 0.02 au; the numbers show the contributions of S_1 in the orbital). Green and blue regions represent the positive and negative orbital phases, respectively.

To explore the self-ECL mechanism of ZL-1, cyclic voltammetry (CV) was researched at the different GCEs.[35–37] From Figure 3F, dual reduction peaks of ZL-1 were discovered at about −1.12 V and −1.50 V in 0.1 M PBS. Correspondingly, a strong first-step ECL signal (ECL1) was presented at −1.22 V, followed by a second-step ECL signal (ECL2) at about −1.60 V (Figure 2B). And just like the CV results, the ECL1 and ECL2 were attributable to the reduction of ZL-1. Furthermore, in terms of the stepping pulse ECL (SP-ECL), the ECL occurrence process that accompanied the changes for components of ZL-1 was revealed. As can be seen in Figure 3H, at the initial stepping potential of 0 V, the ECL transient of ZL-1 was not observed until the second stepping potential was down to – 0.9 V. Powered by the stimulation under potential of −1.3 V, the ECL transient with 4400 a.u. was produced due to the generation of ZL-$1_{Re1}^{\bullet-}$ by the first order reduction of ZL-1. When the final stepping potential was dropped to −1.8 V, the ECL transient enhanced to 7500 au. Because the second-order reduction of ZL-1 happened. Specially, the ECL transient of HNCP without framework structure only reached 770 a.u. when the test potential was −1.3 V, and the ECL intensity was consistent with the test potential of −1.8 V (Figure S8, Supporting Information). Based on these results, the holistic ECL mechanisms of ZL-1 could be speculated: first, the imidazole group in HNCP proceed the cleavage of the N—H bond under alkaline environment to form neutral radical (ZL-1$^{\bullet}$); meanwhile, the ZL-1 was successively reduced at −1.12 V (Re1) and −1.50 V (Re2) to produce the negatively charged anion radicals ZL-$1_{Re1}^{\bullet-}$ and ZL-$1_{Re2}^{\bullet-}$, respectively, which reacted with ZL-1$^{\bullet}$ to form an excited ZL-1_{Re1}* and ZL-1_{Re2}*, accompanied with the energy transfer from HNCP to central Eu ion to achieve ECL1 (−1.22 V) and ECL2 (−1.60 V) emissions. In addition, under higher applying voltage, the second reduction product of ZL-1 reacted with the accumulated first reduction product of ZL-1, accelerating the generation of ZL-$1_{Re1}^{\bullet-}$. This self-enhancement effect was reflected in the ECL intensity-potential curves at 0 ~ −1.3 V and 0 ~ −1.8 V (Figure 2A,B). The ECL mechanism diagram of ZL-1 was shown in **Figure** 4A.

Electron DFT calculation and natural transition orbital (NTO) analysis of the ZL-1 displayed the luminescence mechanism of ZL-1* (ZL-1_{Re1}* and ZL-1_{Re2}*, Figure 4B). The luminescence of ZL-1* is mostly produced by the relaxation of the excited singlet state (S_1) to the ground state (S_0).[10] The transition from NTO 458 to 459 made the major contribution in $S_0 \rightarrow S_1$ of ZL-1. From the change of electron cloud, it can be seen that the luminescence of Eu unit is dominant in ZL-1*, that is antenna effect.[38] Based on the DFT calculations of HNCP energy levels with S_1 and the triplet first excited state (T_1) (Figure S9, Supporting Information), the energy gap ($E_{S_1} - E_{T_1}$) of HNCP is 5202.65 cm^{-1} and the energy difference between T_1 of HNCP and the excited state of Eu^{3+} (E_{T_1}--$E_{Eu^{3+}}$) is 12118.09 cm^{-1}, which fit perfectly with the criteria for antenna effect to occur.[39] Moreover, the occurrence of antenna effect in ZL-1 can also be confirmed experimentally. In Figure S10 (Supporting Information), the UV-vis absorption peaks of ZL-1 at 286 nm and 334 nm exhibited a red shift, and these absorption peaks were attributed to HNCP ligand, indicating the successful coordination of HNCP and Eu(III) ion.[40] In addition, the excitation bands of HNCP centering at 342 and 408 nm red-shifted to 392 and 465 nm due to the coordination process.[41] The emission bands were all from $^5D_0$-^7F_J (J = 1,2,3,4) transitions of Eu^{3+} (592 nm → $^5D_0$-$^7F_1$, 617 nm → $^5D_0$-$^7F_2$, 652 nm → $^5D_0$-$^7F_3$, 687 and 697 nm → $^5D_0$-$^7F_4$, Figure S11, Supporting Information).[19,42] For HNCP ligand, the FL lifetime (λ_{em} = 600 nm) was more transient in ZL-1 (3.74 ns) than in bare HNCP (10.11 ns), but the FL lifetime of Eu^{3+} (λ_{em} = 617 nm) was greatly enhanced in ZL-1 (312.5 µs) than in bare Eu^{3+} (121.0 µs) (Figure S12, Supporting Information). The FL lifetime of coordinated HNCP in ZL-1 was shortened, while the FL lifetime of Eu^{3+} in ZL-1 was increased, indicating energy transfer from HNCP ligand to Eu^{3+} in ZL-1.[43,44] Based on the obtained FL lifetimes, the energy transfer efficiency was calculated as 63%. The above illustrated that the HNCP ligand transferred energy by the non-radiative form from T_1 to the $^5D_0$ energy level of Eu^{3+}, which sensitized the ECL signal production of ZL-1*.

3. Conclusion

In summary, we demonstrated a dinuclear MOF based on $Eu_2(COO)_2$ cluster and HNCP ligand, featuring high self-ECL performance. By means of experiments such as ECL spectra, CV and ECL tests as well as theoretical calculation of DOS and NTO isodensity surfaces in S_1, it was confirmed that the self-ECL mechanism of ZL-1 was composed of three parts: the N—H···π interaction of benzimidazolyl group in HNCP ligand, the two-step reduction induced excitation process of ZL-1, and the antenna effect of HNCP ligand to Eu^{3+}. Remarkably, the ZL-1 possessed significantly enhanced ECL signals and lower ECL potential, and could broaden the pH range of the working environment, which is important for the smart materials design in practical ECL applications to environmental monitoring, biological and cellular immunoassay. This work provides reasonable technical means for revealing the internal ECL mechanism of material, and contributes to a feasible idea of self-assembled self-ECL MOFs by functionalized organic ligands and interactions between central metal ion and ligand.

4. Experimental Section

Synthesis of $[Eu_2(HNCP)_4Cl_4(H_2O)_2]_n$ *(ZL-1)*: 0.1 mmol of $EuCl_3 \cdot 6H_2O$, 0.05 mmol of HNCP, and 0.05 mmol of 2,5-thiophenedicarboxylic acid were dissolved in the mixture of 5 mL acetone and 1 mL H_2O, and then the mixed solution was stirred for 20 min continuously and transferred into Teflon-lined stainless steel autoclave and reacted at 190 °C for 3 days.[45] Finally, the clear light yellow crystals were formed. Anal. Calcd for $C_{40}H_{26}Cl_4Eu_2N_8O_6$ (1160.41). Crystallographic data for the reported crystal structures have been deposited at the Cambridge Crystallographic Data Centre via www.ccdc.cam.ac.uk with 2241093.

Supporting Information

Supporting Information is available from the Wiley Online Library or from the author.

Acknowledgements

This work was supported by the National Natural Science Foundation of China (22274063 and 22274062), the Young Taishan Scholars Program of Shandong Province (tsqn201909124). All of the authors express their sincere thanks.

Conflict of Interest

The authors declare no conflict of interest.

Data Availability Statement

The data that support the findings of this study are available from the corresponding author upon reasonable request.

Keywords

Eu-MOF, Intramolecular Energy Transfer, N—H···π Interaction, self-electrochemiluminescence, two-step reduction

Received: June 21, 2024
Revised: July 15, 2024
Published online:

[1] Z. F. Ding, B. M. Quinn, S. K. Haram, L. E. Pell, B. A. Korgel, A. J. Bard, *Science* **2002**, *296*, 1293.
[2] W. L. Guo, H. Ding, C. Y. Gu, Y. H. Liu, X. C. Jiang, B. Su, Y. H. Shao, *J. Am. Chem. Soc.* **2018**, *140*, 15904.
[3] J. M. Wong, R. Z. Zhang, P. D. Xie, L. Q. Yang, M. L. Zhang, R. X. Zhou, R. Y. Wang, Y. Shen, B. Yang, H. B. Wang, Z. F. Ding, *Angew. Chem., Int. Ed.* **2020**, *59*, 17461.
[4] X. Z. Song, L. Zhao, C. N. Luo, X. Ren, L. Yang, Q. Wei, *Anal. Chem.* **2021**, *93*, 9704.
[5] X. Z. Song, X. J. Li, D. Wei, R. Feng, T. Yan, Y. G. Wang, X. Ren, B. Du, H. M. Ma, Q. Wei, *Biosens. Bioelectron.* **2018**, *126*, 222.
[6] X. Z. Song, X. R. Shao, L. Dai, D. W. Fan, X. Ren, X. Sun, C. N. Luo, Q. Wei, *ACS Appl. Mater. Interfaces* **2020**, *12*, 9098.
[7] A. Zanut, A. Fiorani, S. Canola, T. Saito, N. Ziebart, S. Rapino, S. Rebeccani, A. Barbon, T. Irie, H. Josel, F. Negri, M. Marcaccio, M. Windfuhr, K. Imai, G. Valenti, F. Paolucci, *Nat. Commun.* **2020**, *11*, 2668.
[8] C. Alberoni, G. Pavan, T. Scattolin, A. Aliprandi, *ChemPlusChem* **2024**, 202400142.
[9] L. Z. Hu, G. B. Xu, *Chem. Soc. Rev.* **2010**, *39*, 3275.
[10] D. Zhu, Y. Zhang, S. S. Bao, N. N. Wang, S. Q. Yu, R. G. Luo, J. Ma, H. X. Ju, J. P. Lei, *J. Am. Chem. Soc.* **2021**, *143*, 3S049.
[11] A. F. Irkham, G. Valenti, N. Kamoshida, F. Paolucci, Y. Einaga, *J. Am. Chem. Soc.* **2020**, *142*, 1518.
[12] X. Kuang, Y. C. Luo, R. Kuang, Z. L. Wang, X. Sun, Y. Zhang, Q. Wei, *Carbon* **2018**, *137*, 433.
[13] D. E. Barry, D. F. Caffrey, T. Gunnlaugsson, *Chem. Soc. Rev.* **2016**, *45*, 3244.
[14] D. N. Jiang, C. Huang, J. Zhu, P. Wang, Z. M. Liu, D. Fang, *Coordin. Chem. Rev.* **2021**, *444*, 214064.
[15] Z. C. Yu, J. Tang, H. X. Gong, Y. Gao, Y. Y. Zeng, D. P. Tang, X. L. Liu, *Adv. Funct. Mater.* **2016**, *33*, 2301457.
[16] Y. Gao, M. J. Li, Y. Y. Zeng, X. L. Liu, D. P. Tang, *Anal. Chem.* **2022**, *94*, 13582.
[17] X. Y. Wang, S. Y. Xiao, C. P. Yang, C. Y. Hu, X. Wang, S. J. Zhen, C. Z. Huang, Y. F. Li, *Anal. Chem.* **2021**, *93*, 14178.
[18] Z. C. Jin, X. R. Zhu, N. N. Wang, Y. F. Li, H. X. Ju, J. P. Lei, *Angew. Chem., Int. Ed.* **2020**, *132*, 10532.
[19] H. B. Wei, Z. F. Zhao, C. Wei, G. Yu, Z. W. Liu, B. Zhang, J. Bian, Z. Q. Bian, C. H. Huang, *Adv. Funct. Mater.* **2016**, *26*, 2085.
[20] J. Y. Li, L. D. Wang, Z. F. Zhao, B. X. Sun, G. Zhan, H. Y. Liu, Z. Q. Bian, Z. W. Liu, *Nat. Commun.* **2020**, *11*, 5218.
[21] Y. F. Zhao, D. Li, *J. Mater. Chem. C* **2020**, *8*, 12739.
[22] Y. Y. Ou, W. J. Zhou, Z. C. Zhu, F. K. Ma, R. F. Zhou, F. Su, L. R. Zheng, L. Ma, H. B. Liang, *Angew. Chem., Int. Ed.* **2020**, *59*, 23810.
[23] L. Zhao, X. Z. Song, X. Ren, D. W. Fan, Q. Wei, D. Wu, *Anal. Chem.* **2021**, *93*, 8613.
[24] L. Zhao, M. Wang, X. Z. Song, X. J. Liu, H. X. Ju, H. Q. Ai, Q. Wei, D. Wu, *Chem. Eng. J.* **2022**, *434*, 134691.
[25] J. Alí-Torres, L. Rodríguez-Santiago, M. Sodupe, *Phys. Chem. Chem. Phys.* **2011**, *13*, 7852.
[26] S. Das, D. Saha, S. Karmakar, S. Baitalik, *J. Phys. Chem. A* **2012**, *116*, 5216.
[27] B. Hua, C. Zhang, W. Zhou, L. Shao, Z. D. Wang, L. J. Wang, H. M. Zhu, F. H. Huang, *J. Am. Chem. Soc.* **2020**, *142*, 16557.
[28] F. M. Winnik, *Chem. Rev.* **1993**, *93*, 587.
[29] A. Valdés, J. Brillet, M. Grätzel, H. Gudmundsdóttir, H. A. Hansen, H. Jónsson, P. Klüpfel, G. J. Kroes, F. L. Formal, I. C. Man, R. S. Martins, J. K. Nørskov, J. Rossmeisl, K. Sivula, A. Vojvodic, M. Zäch, *Phys. Chem. Chem. Phys.* **2012**, *14*, 49.
[30] A. Ummadisingu, S. Meloni, A. Mattoni, W. Tress, M. Grätzel, *Angew. Chem., Int. Ed.* **2021**, *60*, 21368.
[31] R. J. Zeng, K. K. Lian, B. Su, L. L. Lu, J. W. Lin, D. P. Tang, S. Lin, X. C. Wang, *Angew. Chem., Int. Ed.* **2021**, *60*, 25055.
[32] R. J. Zeng, Y. L. Li, X. H. Hu, W. J. Wang, Y. X. Li, H. X. Gong, J. H. Xu, L. T. Huang, L. L. Lu, Y. F. Zhang, D. P. Tang, J. B. Song, *Nano Lett.* **2023**, *23*, 6073.
[33] S. K. Bera, P. J. Boruah, S. S. Parida, A. K. Paul, P. Mal, *J. Org. Chem.* **2021**, *86*, 9587.
[34] H. Yamashita, T. Ikezawa, Y. Kobayashi, J. Abe, *J. Am. Chem. Soc.* **2015**, *137*, 4952.
[35] D. Pan, Z. Z. Fang, E. L. Yang, Z. Q. Ning, Q. Zhou, K. Y. Chen, Y. J. Zheng, Y. J. Zhang, Y. F. Shen, *Angew. Chem., Int. Ed.* **2020**, *59*, 16747.
[36] Z. Y. Cao, C. Y. Li, Y. F. Shu, M. Y. Zhu, B. Su, H. Y. Qin, X. G. Peng, *J. Am. Chem. Soc.* **2023**, *145*, 26425.
[37] K. Q. Wu, R. Chen, Z. X. Zhou, X. H. Chen, Y. Q. Lv, J. Ma, Y. F. Shen, S. Q. Liu, Y. J. Zhang, *Angew. Chem., Int. Ed.* **2023**, *62*, e202217078.
[38] R. J. Zeng, L. H. Lin, H. X. Gong, Y. X. Li, J. H. Xu, L. T. Huang, W. J. Wang, S. Lin, D. P. Tang, S. J. Guo, *Chem. Catal.* **2023**, *3*, 100514.
[39] M. D. Ward, *Coordin. Chem. Rev.* **2010**, *254*, 2634.
[40] Z. K. Li, J. L. Gu, S. L. Qi, D. Z. Wu, L. F. Gao, Z. Chen, J. Guo, X. H. Li, Y. Wang, X. M. Yang, Y. F. Tu, *J. Am. Chem. Soc.* **2017**, *139*, 14364.
[41] Y. Q. Wei, Y. F. Yu, K. C. Wu, *Cryst. Growth. Des.* **2007**, *7*, 2262.
[42] M. W. Mara, D. S. Tatum, A. M. March, G. Doumy, E. G. Moore, K. N. Raymond, *J. Am. Chem. Soc.* **2019**, *141*, 11071.
[43] Y. J. Zheng, H. Yang, L. F. Zhao, Y. H. Bai, X. H. Chen, K. Q. Wu, S. Q. Liu, Y. F. Shen, Y. J. Zhang, *Anal. Chem.* **2022**, *94*, 3296.
[44] Y. F. Fang, H. Yang, Y. H. Hou, W. Li, Y. F. Shen, S. Q. Liu, Y. J. Zhang, *Nat. Commun.* **2024**, *15*, 3597.
[45] S. Zhang, Y. Yang, Z. Q. Xia, X. Y. Liu, Q. Yang, Q. Wei, G. Xie, S. P. Chen, S. L. Gao, *Inorg. Chem.* **2014**, *53*, 10952.